MIXING AND FLOW STRUCTURES OF VECTOR-CONTROLLED FREE JETS USING DNS

Koichi TSUJIMOTO

Division of Mechanical Engineering
Graduate School of Engineering, Mie University
1577 Kurimamachiya-cho, Tsu, 514-8507 Japan
tujimoto@mach.mie-u.ac.jp

Koji AO, Toshihiko SHAKOUCHI and Toshitake ANDO
Division of Mechanical Engineering
Graduate School of Engineering, Mie University
1577 Kurimamachiya-cho, Tsu, 514-8507 Japan

ABSTRACT

In order to develop a new mixing procedure, we conduct DNS (direct numerical simulation) of vector controlled free jets. The inflow velocity of jet is periodically oscillated perpendicular to the jet axis. To realize the high accurate computation, a discretization in space is performed with hybrid scheme in which Fourier spectral and 6th order compact scheme are adopted. From visualized instantaneous vortex structures, it is found that the flow pattern considerably changes according to the oscillating frequency, i.e., according to the increasing the frequency, wave, bifurcating and flapping modes appear in turn. In order to quantify mixing efficiency under the vector control, as the mixing measure, statistical entropy is investigated. Compared to the uncontrolled jet, the mixing efficiency is improved in order of wave, flapping and bifurcating modes. So the vector control can be expected for the improvement of mixing efficiency. Further to make clear the reason for the mixing enhancement, Snapshot POD and DMD method are applied. The primary flow structures under the vector control are demonstrated.

Introduction

In order to enhance mixing or diffusion in many industrial applications, jet mixing control has been examined. The control methods used for jet mixing are categorized into either passive or active methods. Irrespective of the method, understanding the mixing state is indispensable for realizing an effective jet control. The results of liner stability analyses reveal that there are two types of dominant modes characterizing the large-scale flow structures near field of a jet, namely, varicose and helical modes, and diffusion or mixing is effectively controlled through these modes. Further, it is well known that a complex jet is made of a combination of these modes (Reynolds et al., 2003). For example, a flapping mode comprises a pair of helical modes with the same frequency and the same amplitude. Further, it is experimentally confirmed that when the axial mode is added to them, a bifurcating jet or a blooming jet is formed (Reynolds et al., 2003). Such an active control was also investigated using DNS (direct numerical simulation) (Hilgers et al., 2001; Silva et al., 2002), and induced the generation of strong diffusion. Although the effectiveness of these active control methods has already been demonstrated thus far, using simple estimations involving the jet width, mean streamwise velocity, turbulence intensity, and so on, it is not well enough to estimate the mixing efficiency using the reliable procedure. In particular, we investigated compound jets (Tsujimoto et al., 2006) and found that their mixing efficiency could not be determined using the simple measure developed for an axisymmetric jet. Therefore, we investigated an appropriate measure for quantifying the mixing efficiency and found that statistical entropy became a good measure (Tsujimoto et al., 2009).

In the present study, from a different view of control method, we focus on the vector control in which an inflow direction varies periodically. In order to investigate the performance of the proposed method, the DNS of axisymmetric jet under the vector control are conducted and the vortical structures are visualized; the mixing efficiency based on the mixing measure are quantified; further to make clear the reason for the mixing enhancement, Snapshot POD and DMD method are applied.

Numerical method

Under the assumption of incompressible and isothermal flow, the dimensionless governing equations are as follows:

$$\frac{\partial u_i}{\partial x_i} = 0 \qquad (1)$$

$$\frac{\partial u_i}{\partial t} + h_i = -\frac{1}{\rho}\frac{\partial p}{\partial x_i} + \frac{1}{Re}\frac{\partial^2 u_i}{\partial x_j \partial x_j} \qquad (2)$$
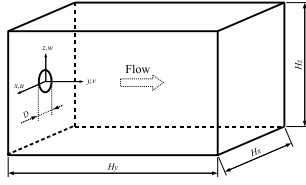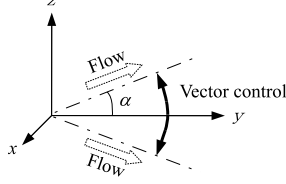
1

Figure 1. Coordinate system and computational domain

Figure 2. Definition of inflow condition

Table 1. Calculation conditions of vector controlled jets

	fine	coarse
Domain	$20D \times 30D \times 20D$	
Grid number	$256 \cdot 300 \cdot 256$	$128 \cdot 150 \cdot 128$
Re number	$Re = V_0 D/\nu = 1500$	
Prl number	$Pr = \nu/\alpha = 0.707$	
Frequency condition	0.000, 0.010, 0.040, 0.400	0.030, 0.032, 0.035, 0.038, 0.100, 0.180, 0.200, 0.250, 0.280, 0.330, 0.350
Max angle	$\alpha_0 = 5$	

$$(h_i = \varepsilon_{ijk}\omega_j u_k, \ \omega_j : \text{vorticity})$$

$$\frac{\partial T}{\partial t} + \frac{\partial u_i T}{\partial x_i} = \frac{1}{RePr}\frac{\partial^2 T}{\partial x_i \partial x_i} \qquad (3)$$

The nonlinear terms are expressed in the rotational form to conserve the total energy; therefore, p represents the total pressure. For the characteristic length and velocity, the nozzle diameter D and the streamwise velocity $V_0 = V_1 - V_2$ (V_1, V_2 refer to Eq. (4)) were chosen for nondimensionalization, respectively. The Reynolds number is defined as $Re = V_0 D/\nu$ (ν: kinematic viscosity). A Cartesian coordinate system is employed in which y is the streamwise direction and x and z are the lateral directions. Spatial discretization is performed using a hybrid scheme that adopts a sixth-order compact scheme (Lele, 1992) in the streamwise direction and a Fourier series in the lateral directions. In order to remove the numerical instability due to the nonlinear terms, the 2/3-rule is applied to the lateral directions, and implicit filtering is carried out for the streamwise direction using the sixth-order compact scheme. A third-order Adams-Bashforth method is used for time advancement. The well-known MAC scheme is employed for pressure-velocity coupling, which generates a Poisson equation for the pressure. After the Poisson equation is Fourier transformed in the x and z directions, independent differential equations are obtained for each wave number and then discretized using the sixth-order compact scheme. Finally, a pentadiagonal matrix is deduced for each wave number. In the present simulation code, the matrix is solved using the LU decomposition method. The outflow boundary condition is introduced for both the momentum and the energy equations by solving the simplified convective equations

Calculation conditions

Figure 1 shows a schematic of the flow field. The inlet velocity distribution is assumed to be top-hat type, which is defined as follows:

$$V_b(r) = \frac{V_1 + V_2}{2} - \frac{V_1 - V_2}{2}\tanh\left[\frac{1}{4}\frac{R}{\theta_0}\left(\frac{r}{R} - \frac{R}{r}\right)\right] \qquad (4)$$

where V_1 and V_2 are the center velocity and co-flow velocity, respectively. θ_0 denotes the initial momentum thickness. r is the distance from the jet axis, and $R(= D/2)$ is the radius of the inlet jet. These parameters are selected by referring to the literature [3]: $V_1 = 1.075V_0$, $V_2 = 0.075V_0$, and $R/\theta_0 = 20$. The following thermal boundary conditions are assumed: the ambient temperature is constant at T_0 and the inflow temperature is T_1 at the region where the absolute value of the inflow velocity is larger than V_2. Computational conditions such as the size of computational domain, the Reynolds number, the Prandtl number are $(H_x, H_y, H_z) = (20D, 30D, 20D)$, $Re = 1500$ and $Pr = 0.71$, respectively. The grid number is $(N_x, N_y, N_z) = (256, 300, 256)$ for a fine case, $(N_x, N_y, N_z) = (128, 150, 128)$ for a coarse case. The statistical properties are averaged over the time. The mean quantity is denoted with bar ($-$) and fluctuating components, by prime ($'$).

In the present calculation, as shown Fig.2, the inflow direction varies along z direction so that the inflow condition mimics vector control. Further, to maintain a constant rate of inflow in the computational volume, the inflow velocity component is estimated as follows:

$$
\begin{aligned}
u(x,0,z) &= u_{rad} \\
v(x,0,z) &= V_b(r)\cos(\alpha) + v_{rad} \\
w(x,0,z) &= -V_b(r)\sin(\alpha) + w_{rad}
\end{aligned} \qquad (5)
$$

$$\left(r = \sqrt{x^2 + (z\cos(\alpha))^2}, \ \alpha = \alpha_0 \sin(2\pi ft)\right)$$

where r is the distance from the jet center line. α is the inclination angle shown in Fig.2, and α_0 (=5°) is the maximum inclination angle. f is the oscillating frequency. In the above equations, a random perturbation $(u_{rad}, v_{rad}, w_{rad})$ with 1% of the strength of V_0 is superposed on the inflow mean velocity. The calculation conditions are summarized in Table 1.
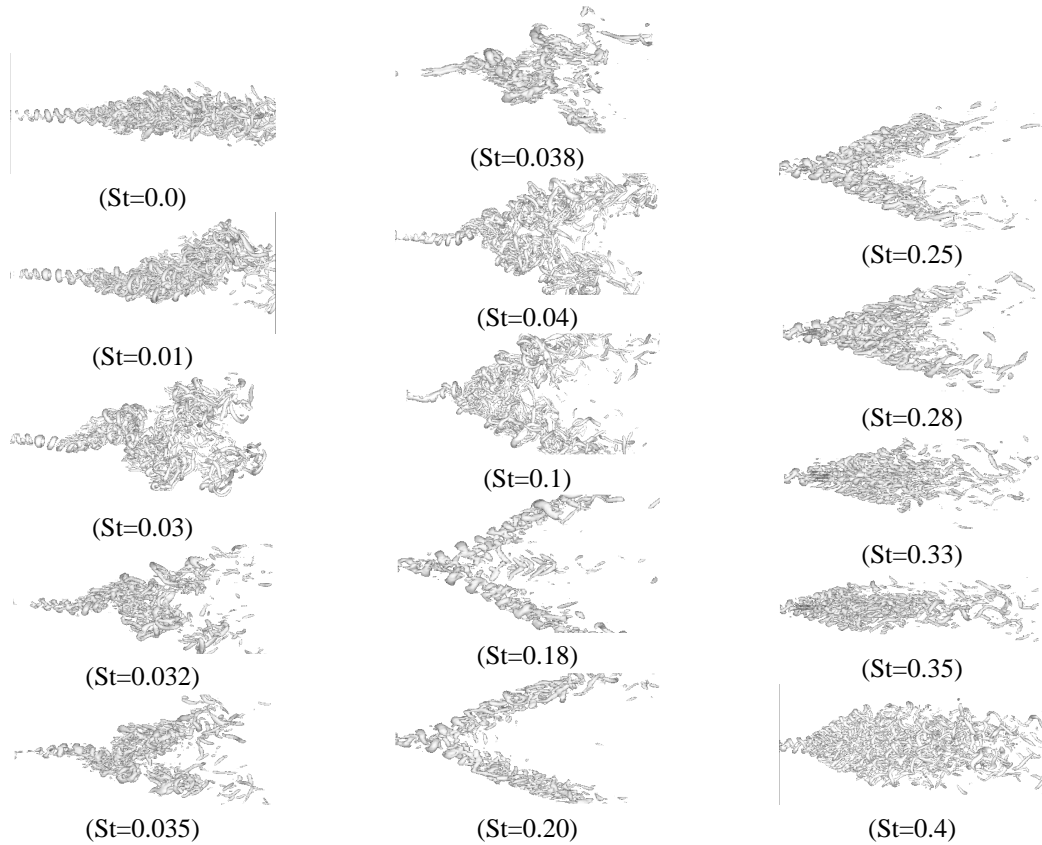
2

Figure 3. Instantaneous vortex structures ($Q = 0.05$) at various St numbers

Results and discussions
Vortical structures

In order to investigate the effect of the oscillating frequency, the isosurface of the second invariance of the velocity gradient tensor, Q (=0.05), is visualized from a perpendicular view to the oscillating plane, as shown in Figs.3. Although the oscillating angle at the inflow position is small, *i.e.*, $\alpha_0 = 5°$, the controlled jets ($St \neq 0$) spread downstream with an angle larger than the oscillating angle. In the uncontrolled case ($St = 0$), the vortex rings are formed upstream (left side of each figure), and then, they break down and entangled tube structures appear downstream. Further, with increasing oscillating frequency, the flow pattern changes considerably: at $St = 0.01$, although the fine-scale structure is similar to that of the uncontrolled case, a large-wavelength oscillation occurs downstream, and hereafter, this pattern is called the wave mode. At $St = 0.03$, although the wavelength is shorter than that at $St = 0.01$, the wave mode is retained. At $St = 0.032$ and 0.035, the wave mode is blurred. At $St = 0.04$, a bifurcating mode, in which the jet separates into two distinct components begins to appear; at $St = 0.1$, the bifurcating mode is stable. At $St = 0.18$ and 0.2, the bifurcating mode is markedly enhanced. At $St = 0.25$, the vortices are generated downstream between the two separated jets. At $St = 0.28, 0.33, 0.35$, and 0.40, this tendency of generation of vortical structures continues irrespective of the St value. At $St = 0.4$, after flowing from the nozzle, strong hair-pin-like structures are alternately formed upstream. These structural features are similar to the flapping excitation observed in our previous studies [5] and other results [3]. In the present paper, this pattern is called the flapping mode. The above mentioned results show that the wave mode is predominant at the low St values, the bifurcating mode is predominant at medium St values, and the flapping mode is predominant at high St values. It should be noted that in the previous research[2],[5],[6], a strong axial disturbance in the axial direction and a weak disturbance in the azimuthal direction were added at the jet nozzle exit resulting in the generation of the bifurcating mode; however, our proposed method is also capable of producing a similar flow mode. In addition, by varying the oscillating frequency, the vector control method is capable of easily controlling the flow mode. Hereinafter, we focus on the fine-resolution data at $St = 0.01, 0.04$, and 0.4 and investigate the flow properties and mixing efficiency at these St values.

Mixing characteristics

In order to quantify the mixing state, Everson et al.(1998)investigated the statistical entropy based on the passive scalar concentration, and they demonstrated the characteristics of this measure by examining the experimental data. As well as we validate this mixing measure based on the DNS data of active controlled jet (Tsujimoto et al., 2009) In the following, we provide a simple explanation of this measure.
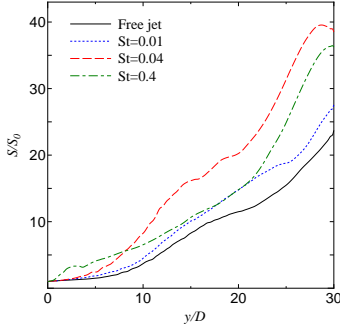
Boltzmann proposed the statistical entropy, which is de-

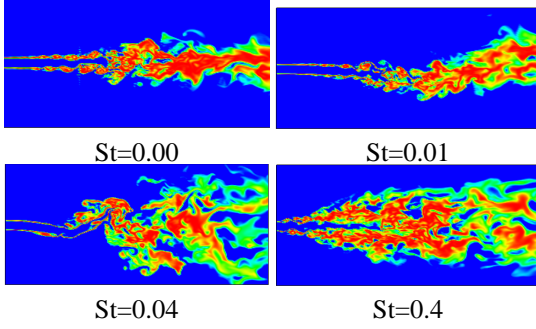Figure 4. Mean the statistical entropy distribution

St=0.00   St=0.01
St=0.04   St=0.4

Figure 5. Contour of statistical entropy on the y-z plane through the jet centerline.

fined as the logarithm of combination, W.

$$S = k \ln W \qquad (6)$$

where k is the Boltzmann constant. W is the combination of the number of molecules in the i-th coarse-grained cell, N_i, namely, $W = \frac{N!}{N_1! N_2! \cdots N_M!} = \frac{N!}{\prod N_i!}$. Since incompressible flow is assumed in the present study, the temperature can be related to the concentration of the passive scalar, *i.e.*, $\phi = (T - T_2)/(T_1 - T_2)$. Considering the small volume surrounding a grid point i, $\Delta V (= \Delta_x \Delta_y \Delta_z)$, the number of molecules is denoted by $N_i = \phi_i \Delta V$; therefore,

$$S = k\Delta V \left[\Phi \ln \Phi - \sum_{i=1}^{M} \phi_i \ln \phi_i \right] \qquad (7)$$

where $\Phi = \sum \phi_i$

In order to investigate the streamwise variation of the statistical entropy, S is summed over the plane perpendicular to the streamwise direction, and $\bar{S}$ is defined as S normalized with the inflow quantity, S_0. M represents the number of grids on the $x - z$ plane; $M = 65,536 (= 256 \times 256)$. As shown in Fig. 4, the statistical entropy increases downstream in the order of the wave-, flapping-, and bifurcating cases. This is reflected in the increase of randomness downstream and the mixing enhancement due to the vector control. When a larger

total number of molecules exist in space, the statistical entropy is greater. In other words, this measure reflects the physical property corresponding to the jet expansion. However, if the same number of molecules is distributed between different jets, the first terms of Eq. (7) does not represent the difference concerning the mixing property; thus it seems that the second term of Eq. (7) includes the substantial properties for mixing, despite the fact that the magnitude of this term is smaller than that of the first one. From this reason, in our previous paper (Tsujimoto et al., 2009), we visualized the $\phi_i \ln \phi_i$, and found that the high-value region corresponds to the mixing region. In order to determine the location of the highly mixed region, the local mixing measures is visualized. Figures 5 show the iso-contours of the component of fluctuating entropy, $\phi_i \ln \phi_i$, on the $y - z$ plane through the jet centerline. In all cases, the fluctuating entropy is strong in the region where a strong upstream shear layer is related to the vortical structures. Further downstream, corresponding to the extension of jet diffusion, the distribution of the fluctuating entropy also spreads in the ambient,and unlike the distribution of the passive scalar, the mixing region is well visualized using the fluctuating entropy.

Extracted structures with Snapshot POD method

So far statistical extractions of structures from various turbulent flows are conducted using POD (proper orthogonal decomposition) method. When the conventional POD is applied to three-dimensional problems, a huge eigenvalue problem which is not substantially not resolved, occurs. To avoid this problem, Snapshot POD (SPOD) method has been proposed by Sirovich (1987). In the present study, in order to investigate the dynamics of flow structures under the vector control, SPOD method is is introduced. The SPOD method is simply explained as follows:

It is assumed that a fluctuating velocity field is represented with eigenfunctions,$\boldsymbol{\phi}_i(\boldsymbol{x})$ and random coefficients, $a_i(t)$.

$$\boldsymbol{u}'(\boldsymbol{x},t) = \sum_{i=1}^{N} a_i(t) \boldsymbol{\phi}_i(\boldsymbol{x}) \qquad (8)$$

The eigenfunctions$\boldsymbol{\phi}_i(\boldsymbol{x})$ and $a_i(t)$ is substituted into a original integral equation of the conventional POD method, the following equation is obtained.

$$C_{mn} a_i^n = \lambda_i a_i^m \qquad (9)$$

where λ_i is the i-th eigen value，a_i^n is the i-th eigenvector, C_{mn} is two temporal correlation tensor defined as follows:

$$C_{mn} = \frac{1}{N} \int \int \int_V \boldsymbol{u}(\boldsymbol{x},t_m) \boldsymbol{u}(\boldsymbol{x},t_n) d\mathbf{x} \qquad (10)$$

The eigenvalue problem of Eq.(9) is solved and the eigenfunctions are obtained.

$$\boldsymbol{\phi}_i(\boldsymbol{x}) = \frac{1}{N\lambda_i} \sum_{n=1}^{N} a_i^n \boldsymbol{u}(x,t_n) \qquad (11)$$

(a) normal mode(St=0.0)

(b) wavy mode(St=0.01)

(c) bifurcating mode(St=0.04)
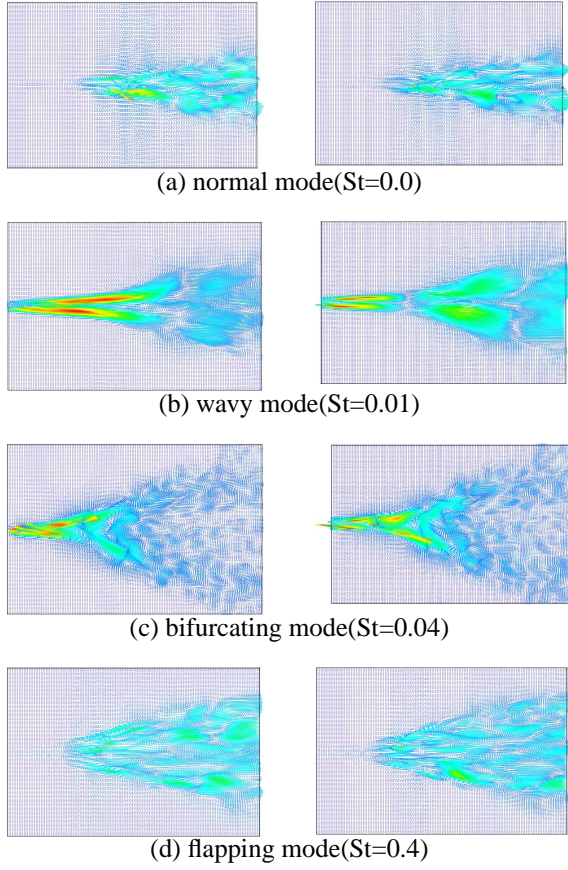

(d) flapping mode(St=0.4)

Figure 6. Vector plots of eigenfunction (left column: 1st mode; right column: 2nd mode)

In the POD method, it is well-known that the magnitude of eigenvalues relate to the energy of the fluctuating velocity. Hereinafter the eigenfunctions are arranged in the order of increasing eigenvalues. The maximum and next eigenvalue called as 1st and 2nd mode.

Figures 6 show the vector plots of eigenfunction in $y - z$ plane through the centerline. The pattern of both 1st and 2nd mode demonstrate a similar trend with a certain phase-shift, these mode contribute to the low-dimensional dynamics in pairs. From Fig.6(a)(d), both the uncontrolled and the flapping mode distribute downstream, suggesting that the vector control influences indirectly on these mode. On the other hand, for the low frequency case, the large-scale mode related to the vector control is predominant upstream. Since the SPOD method extracts the flow mode on the basis of the fluctuating energy, the mode is related to the region where the time-averaged fluctuating energy is strong. Thus, the upstream part of both the wavy and bifurcating mode is attributed to the occurrence of pseudo turbulence due to the vector control. In addition, it is found that the small-scale motion in the separated region of bifurcating jet contributes to a enhancement of scalar mixing.

Extracted structures with DMD method

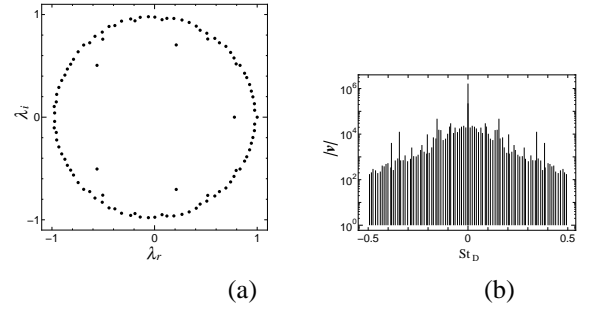Recently as a new analysis tool, DMD (Dynamic mode decomposition) method is proposed by Schmid (2010). Dif-

(a)   (b)

Figure 7. Distribution of (a) eigenvalues and (b) eigenvectors
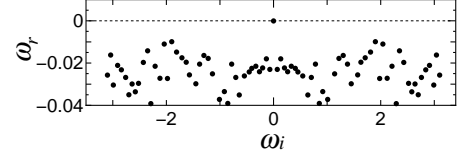

Figure 8. Distribution of eigenmode(ω)

ferently to the POD method, since the DMD is easily capable of extracting the temporally periodic mode, thus it is considered that this method is useful to examine the dynamics under the vector control. The DMD method is simply explained as follows: For the velocity field $\boldsymbol{u}_m = \boldsymbol{u}(\boldsymbol{x}, t_m)$ it assumes a linearized relationship between time steps

$$\boldsymbol{u}_m = \boldsymbol{A}\boldsymbol{u}_{m-1} \tag{12}$$

Since it needs a huge computer power to directly solve the eigenvalue problem of matrix $\boldsymbol{A}$, Companion matrix, $\boldsymbol{C}$ which approximates $\boldsymbol{A}$, is introduced.

$$\boldsymbol{u}_m = \boldsymbol{A}\boldsymbol{u}_{m-1} = c_0\boldsymbol{u}_0 + \cdots + c_{m-1}\boldsymbol{u}_{m-1} = \boldsymbol{K}\boldsymbol{c} \tag{13}$$
$$\boldsymbol{A}\boldsymbol{K} = \boldsymbol{K}\boldsymbol{c} \tag{14}$$

where $\boldsymbol{K} = [\boldsymbol{u}_0, \boldsymbol{u}_1, \cdots \boldsymbol{u}_{m-1}], \boldsymbol{c} = [c_0, \cdots, c_{m-1}]$ Solving the eigenvalue problem of matrix $\boldsymbol{C}$, its eigenfunction is obtained:

$$\boldsymbol{C} = \boldsymbol{T}^{-1}\boldsymbol{\Lambda}\boldsymbol{T} \tag{15}$$

$\boldsymbol{T}$ is the eigenvector of matrix $\boldsymbol{C}$, $\boldsymbol{T}^{-1}$ is the inverse one. Also the eigenvalue of $\boldsymbol{C}$, i.e., $\boldsymbol{\Lambda} = diag(\lambda_1, \ldots, \lambda_m)$ are the primly part of the eigenvalue of $\boldsymbol{A}$. Finally, the eigenvectors of $\boldsymbol{A}$, $\boldsymbol{V}$ are given by this equation.

$$\boldsymbol{V} = \boldsymbol{K}\boldsymbol{T}^{-1} \tag{16}$$

Figure 7(a) shows the plots of the eigenvalue of uncontrolled jet using the DMD method. The eigenvalue λ is a complex number and all one distribute on the unit circle. Figure 7(b) is the magnitude of eigenvalues. In the fig., the abscissa axis is the Strouhal number $\mathrm{St}_D (= \Im[\omega_i]D/2\pi V_0)$ defined with $\omega_i = \left(\frac{\log \lambda_i}{\Delta t}\right)$. The strength of mode depends on

5

(a) normal mode($St = 0.0, St_D \approx 0.302$ mode)

(b) wavy mode($St = 0.01, St_D \approx 0.00993$ mode)

(c) bifurcating mode($St = 0.04, St_D \approx 0.0399$ mode)

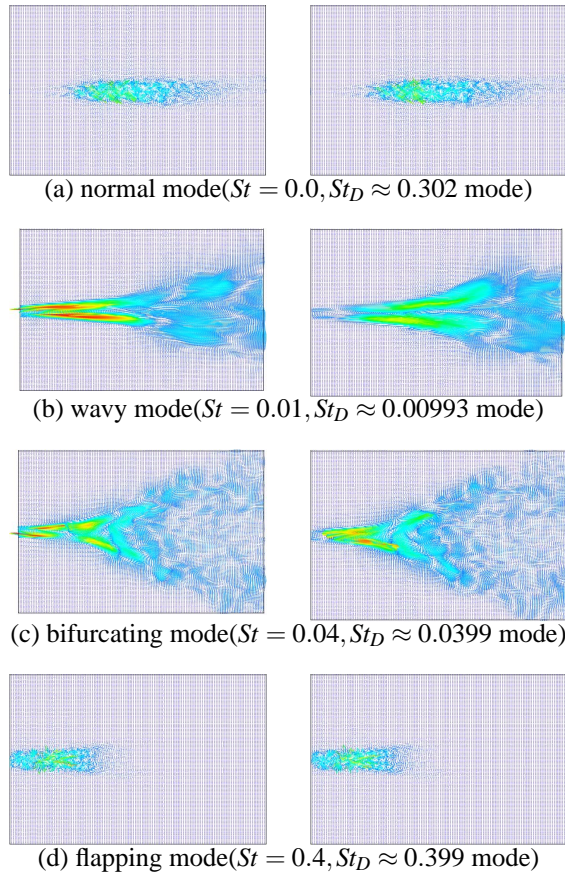(d) flapping mode($St = 0.4, St_D \approx 0.399$ mode)

Figure 9.   Vector plots of unstable mode extracted with DMD nethod (left column: imaginaly part mode; right column: real parte)

the Strouhal number and increases with decreasing the frequency. Figure 8 shows the map of ω of the uncontrolled jet. In the Fig. ω_r is the real part of ω, that means the rate of amplification; ω_i is the imaginary part, which corresponds to the temporal frequency. It should be noted that when the ω_r approaches zero, the mode tends to stably exist among all mode, *i.e.*, the mode nearest to $\omega_r = 0$ is defined as a dominant dynamic mode. From Fig.8 the dominant dynamic mode of the uncontrolled jet, $\omega_i \approx 1.9$. Here, the Strouhal number is estimated from this value , $St_D \approx 0.302$. Namely, it founds that this value corresponds to the preferred mode($0.25 < St_p < 0.5$). For the wavy, the bifurcation, and the flapping mode, the Strouhal number of the dominant dynamic mode, is $St_D \approx 0.00993, 0.0399, and 0.399$, respectively. It is interesting to note that the dominant dynamic mode quit agree well with the frequency of vector control.

Figures 9 show the vector plots of eigenfunction of the dominant dynamic mode. Similar to the relation of 1st and 2nd mode of SPOD, the pattern of both real and imaginary part of dynamic mode demonstrate a similar trend with a certain phase-shift. From Fig.9(a), corresponding to the preferred mode of uncontrolled jet, the small-scale mode are formed

around the broken down of the potential core. The wavy and bifurcating mode in Fig.9(b)(c) demonstrate the large-scale pattern upstream and the similar to the 1st and 2nd mode of SPOD in Fig.6(b)(c). For the flapping mode, the small-scale mode due to the vector control appears upstream region as well as other controlled mode.

Conclusions

In order to improve the mixing performance of free jet, the vector control as the useful method is proposed. As the control parameter, the oscillating frequency varies, and the flow and scalar field are investigated. Conclusions are as follows:

1. From the instantaneous view of flow field, it is found that according to the increasing of oscillating frequency, wavy, bifurcating and flapping mode appear in turn. It suggests that the changing oscillating frequency is capable of controlling easier the flow state.
2. From the mixing measures using the statistical entropy, it is found that the mixing efficiency is improved in order of the wave-, the flapping- and the bifurcating mode compared to the uncontrolled jet.
3. Using Snapshot POD method and DMD method, the primary flow structures under the vector control is demonstrated, in particular, it founds that the frequency of the dominant dynamic mode quite agree well with the control frequency.

REFERENCES

Hilgers, A., and Boersma, B. J., "Optimization of turbulent jet mixing", 2001, *Fluid Dyn. Res.*, Vol. 29, pp. 345-368.

Everson, R., Manin, D., and Sirovich, L., 1998, "Quantification of Mixing and Mixing Rate from Experimental Observations", *AIAA J.* , Vol. 36, pp. 121-127.

Lele, S. K., 1992, "Compact finite difference schemes with spectral-like resolution", *J. of Comp. Phys.* Vol. 103, pp. 16-42.

Reynolds, W. C., Parekh, D. E., Juvet, P. J. D., and Lee, M. J. D., 2003, "Bifurcating and Blooming Jets", *Annu. Rev. Fluid Mech.*, Vol. 35, pp. 295-315.

Schmid, S. J., 2010, "Dynamic mode decomposition of numerical and experimental data", *J. Fluid Mech.*, Vol. 656, pp. 5-28.

Silva, C. B., and Metais, O., 2002, "Vortex control of bifurcating jets: A numerical study", *Phys. of Fluids*, Vol. 14, pp. 3798-3819.

Sirovich, L., 1987, "Turbulence and the dynamics of coherent structures", *Q. Appl. Math.* Vol. 45, pp. 561-590.

Tsujimoto, K., Shakouchi, T. Sasazaki, S., and Ando, T., 2006, "Direct Numerical Simulation of Jet Mixing Control Using Combined Jets", *JSME Int. J. Ser. B*, Vol. 49-4, pp. 966-973.

Tsujimoto, K., Kariya, S., Shakouchi, T., and Ando, T., 2009. "Evaluation of jet mixing rate based on DNS data of excitation jets", *Int. J. Flow Control*, Vol. 1-3, pp. 213-225.